Trafficability Analysis for Lunar/Planetary Exploration Rover using Thrust-Cornering Characteristic Diagram

Genya Ishigami, Keiji Nagatani, and Kazuya Yoshida

***Abstract*— In this paper, a trafficability analysis for the exploration rover is described. A rover driving on loose terrain often experiences its slippages (wheel slips or vehicle sideslip), and in particular, these slips become larger when the rover traverses on a slope of loose sand. The authors have investigated traction mechanics of a rigid wheel of the rover on loose terrain to deal with the slipping behavior of the wheel. In this paper, based on our previous works regarding the wheel-terrain interaction, we propose a Thrust-Cornering Characteristics Diagram in order to analyze the trafficability of the rover on sandy slopes. The thrust-cornering characteristics diagram is composed of various characteristics curves of wheel forces, namely thrust and cornering forces, for various wheel slippages. This diagram provides quantitative criteria for slope traversing capability of the rover on arbitrary angles of slope. The usefulness of the proposed diagram for the trafficability analysis is confirmed through slope traversal experiments using a four-wheel test bed. Further, possible application using the thrust-cornering characteristics diagram for steering maneuver to traverse a slope is presented.**

I. INTRODUCTION

The surface mobility using wheeled mobile robots (Rovers) is one of the important technologies for lunar/planetary exploration missions. The rover has to have enough capabilities to travel highly challenging terrains, climb or traverse slopes around craters on the target body. As demonstrated by NASA/JPL Mars Exploration Rovers, a wheel slippage of the rover is one of the particular disturbances when the rover traveled on sandy terrain [1]. A vehicle of a rover will also experience skidding behavior due to the dynamic slips generating between wheel and loose terrain. In addition, it is easily deduced that the wheel slippage increases when a rover climbs or traverses sandy slopes. Therefore, investigation about the dynamic wheel-terrain interaction is necessary for better analysis of the trafficability of the rover on sandy slope, since the relationship between wheel traction forces and traction load due to the gravity determines the trafficability of the rover.

The mechanics of the slipping wheel on loose terrain has been investigated in the field of terramechanics, as in [2]-[4]. For instance, analysis of wheel-soil interaction mechanism and modeling of stress distributions underneath a wheel have been well studied in [2][3]. We have also elaborated a wheel-soil contact model, which is able to deal with steering motion characteristics of planetary rovers on loose terrain [4].

This work was supported in part by Research Fellowships of the Japan Society for the Promotion of Science for Young Scientists.

The authors are with Department of Aerospace Engineering, Tohoku University, Aoba 6-6-01, Sendai, 980-8579, Japan, {ishigami,keiji,yoshida}@astro.mech.tohoku.ac.jp

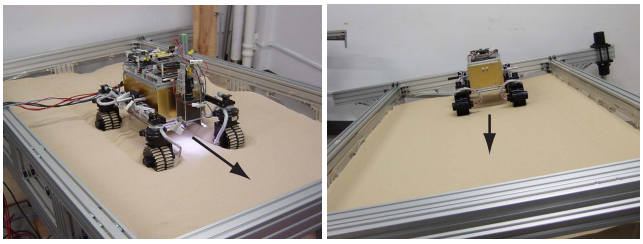

(a) Slope climbing (b) Slope Traversing

Fig. 1. Definition of slope climbing/traversing cases

The slope climbing (Fig. 1-(a)) capability of the rover has been discussed in a plenty of researches [5]-[7]. Seraji proposed a traversability index as a measure for rover's traversability on planetary surfaces. This index was expressed by linguistic fuzzy sets that quantify the suitability of the terrain for traversal based on its physical properties, such as slope and roughness [5]. Kuroda et al. conducted slope climbing experiment of a rover by changing gravitational acceleration with considering a similarity model for the rover [6]. However, analytical criteria to determine the slope traversing (Fig. 1-(b)) capability of the rover are still left as an open issue. To deal with the slope traversing behavior is relatively complicated because the rover makes steering maneuvers to traverse a slope and then wheels generates both longitudinal and lateral forces.

In this paper, we propose a diagram for the trafficability analysis of a rover traversing on sandy slopes, based on the wheel model developed in our previous work as in [4], As noted above, there are two wheel forces, which should overcome a traction load of a vehicle, are generated to achieve successful slope traversing. One of the wheel forces is Thrust force and the other is Cornering force. These two forces are characterized by wheel slippages (longitudinal and lateral slips of wheel). Then, we came up with that combining these characteristics with correspond to wheel slippages provides an analytical diagram for the trafficability analysis. In this research, this diagram is named as *Thrust-Cornering Characteristics Diagram*. Using the diagram, slope traversable or untraversable conditions can be quantitatively determined. The usefulness of the proposed diagram for the trafficability analysis is confirmed through slope traversal experiments using a four-wheel test bed on a tiltable test field covered with loose sand. Further, possible application using the thrust-cornering characteristics diagram for steering maneuver of the rover is presented.

This paper is organized as follows. Section II describes criteria for slop traversing capability and then the relationship

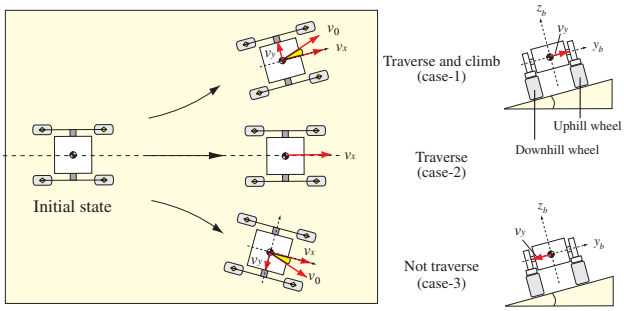

Fig. 2. Slope traversing case: traversable and untraversable

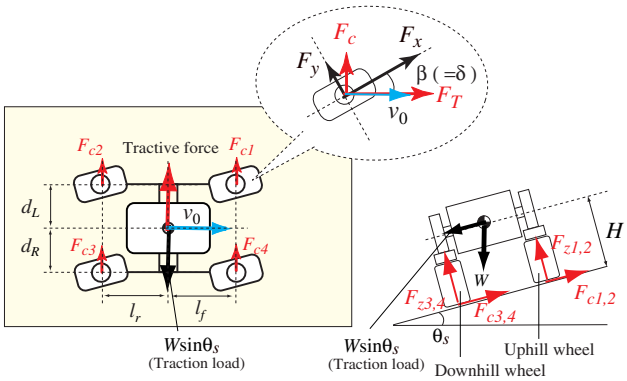

Fig. 3. Force balance on slope traversing case

between both thrust/cornering forces and the criteria is presented. In Section III, the analytical model for wheel force is introduced to address the thrust and cornering forces. Then, the proposed Thrust-Cornering Characteristics Diagram is described in Section IV along with experimental validation of the proposed diagram. Section V deals with the possible application using the proposed diagram.

II. SLOPE TRAVERSING CRITERIA

In this section, first, the definition of slope traversing is described. Then, criteria for the slope traversing capability are addressed.

A. Definition of Traversable and Untraversable

When a rover traverses along with a slope in sideway as shown in Fig. 2, the rover mainly behaves mainly three cases: 1) traverse and climb (positive lateral velocity of vehicle, $+v_y$), 2) traverse (along with straight line, $v_y = 0$), and 3) not traverse (or slide to downside, negative lateral velocity of vehicle, $-v_y$). This research assumes that 1) and 2) are defined as traversable (successful traverse) cases, whereas 3) is an untraversable case. Then, in order to successfully traverse a slope, the lateral velocity of vehicle should be greater than or equal to zero.

B. Criteria for Slope Traversing Capability

An analysis of a slope climbing of a rover is simply determined by a uniaxial force balance between drawbar pulls (longitudinal forces) of wheels and a vehicle's traction load due to the gravity. However, when the rover traverses a sandy slope, the wheel generates not only longitudinal force but also lateral force since the rover makes steering maneuvers to traverse a slope.

Focusing on the force balance between the tractive force and vehicle traction load as shown in Fig. 3, the tractive forces should be larger than the traction load in order to achieve the slope traversing. Here, it is obvious that wheels originally generate this tractive force of vehicle.

Fig. 3 also describes a schematic figure regarding the force balance of wheel. When the vehicle traverses a slope, a sideslip of wheel can be observed. This slippage into lateral direction of wheel is measured by slip angle β. The detail of the slip angle is explained in Section III, later. Because of this sideslip, the wheel generates lateral force named Side force F_y. It can be clearly seen that tractive force of vehicle is composed of a summation from F_{c1} to F_{c4}, which are cornering forces of each wheel. The cornering force F_c is given as a couple of drawbar pull F_x and side force F_y:

$$F_c = F_x \sin\beta + F_y \cos\beta \tag{1}$$

From the above, the rover can traverse when a summation of cornering forces overcomes the traction load $W \sin\theta_s$. Therefore, one of criteria for the slope traversing capability is therefore determined as follows:

$$(F_{c1} + F_{c2} + F_{c3} + F_{c4}) \geq W \sin\theta_s \tag{2}$$

On the other hand, another wheel force, F_T, can be composed as seen in Fig. 3. In this research, F_T is named as *Thrust force* consisting of drawbar pull and side force:

$$F_T = F_x \cos\beta - F_y \sin\beta \tag{3}$$

The thrust force should be greater than zero so that the rover can travel the slope ahead. Then, another criteria is simply defined as:

$$F_{T1} = F_{T2} = F_{T3} = F_{T4} \geq 0 \tag{4}$$

C. Force Equilibrium Point

There is an equilibrium point where the traction load is equal to a summation of cornering forces and then, the rover can traverse a slope along with straight line at this force equilibrium point. (This situation is case-2) as shown in Fig. 2.) The force equilibrium can be written as follows:

$$(F_{c1} + F_{c2} + F_{c3} + F_{c4}) = W \sin\theta_s \tag{5}$$

Here, assuming that the ratio of the required cornering force of each wheel, F_{c1} to F_{c4}, is equivalent to the ratio of the vertical force of each wheel, F_z, the following equation can be obtained:

$$F_{c1} : F_{c2} : F_{c3} : F_{c4} = F_{z1} : F_{z2} : F_{z3} : F_{z4} \tag{6}$$

note that $(F_{z1} + F_{z2} + F_{z3} + F_{z4}) = W \cos\theta_s$. Then, from (5) and the above equation, the required cornering force of

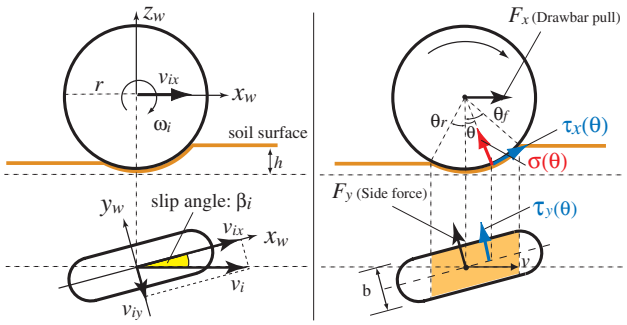

Fig. 4. Analytical model for wheel force

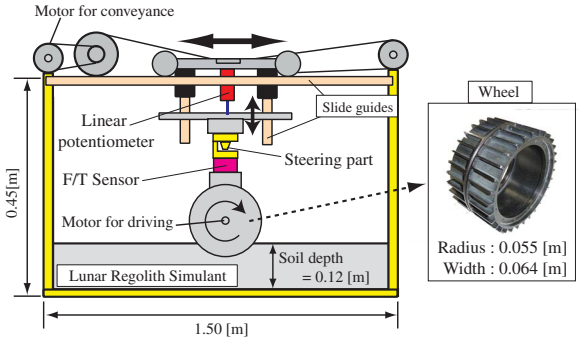

Fig. 5. Schematic view of single wheel test bed

each wheel can be calculated as follows:

$$\left.\begin{aligned} F_{c1} &= \frac{W\sin\theta_s}{(1+l_f/l_r)\cdot(1+d'_L/d'_R)} \\ F_{c2} &= \frac{W\sin\theta_s}{(1+l_r/l_f)\cdot(1+d'_L/d'_R)} \\ F_{c3} &= \frac{W\sin\theta_s}{(1+l_r/l_f)\cdot(1+d'_R/d'_L)} \\ F_{c4} &= \frac{W\sin\theta_s}{(1+l_f/l_r)\cdot(1+d'_R/d'_L)} \end{aligned}\right\} \quad (7)$$

where, $d'_L = (d_L\cos\theta_s + H\sin\theta_s)$, $d'_R = (d_R\cos\theta_s - H\sin\theta_s)$; l_f and l_r are wheelbase; d_L and d_R are tread; and H is a height of the centroid of the vehicle.

III. CHATACTERISTICS OF WHEEL FORCES

As indicated in (1) and (3), to clarify characteristics of cornering force and thrust force, it is needed to know characteristics of drawbar pull F_x and side force F_y. In this section, an analytical model of forces around slipping wheel are introduced based on our previous works as in [4]. First, wheel coordinate system is defined and then parameters for wheel slippages into longitudinal and lateral direction are presented. Equations for drawbar pull and side force are then described. The analytical model of wheel force is verified using single wheel experiment.

The following analysis concerns a rigid wheel rotating on loose soil. A wheel coordinate system is defined using a right-hand frame, as shown in Fig. 4; in this system, the longitudinal direction is denoted by x, the lateral direction by y, and the vertical direction by z. The coordinate frame rotates according to the steering action of the wheel (the yaw rotation around the z axis) but does not rotate with the driving motion of the wheel (the pitch rotation around the y axis).

A. Slip ratio and Slip angle

Slips are generally observed when a rover travels on loose sand. In particular, during steering or slope-traversing maneuvers, slips in the lateral direction are also observed. The slip in the longitudinal direction is expressed by the slip ratio s, which is defined as a function of the longitudinal traveling velocity of the wheel v_x and the circumference velocity of the wheel $r\omega$ (r is the wheel radius and ω represents the angular velocity of the wheel).

$$s = \begin{cases} (r\omega - v_x)/r\omega & (|r\omega| > |v_x| : \text{driving}) \\ (r\omega - v_x)/v_x & (|r\omega| < |v_x| : \text{braking}) \end{cases} \quad (8)$$

The slip ratio assumes a value in the range from -1 to 1.

On the other hand, the slip in the lateral direction is expressed by the slip angle β, which is defined by v_x and the lateral traveling velocity v_y as follows:

$$\beta = \tan^{-1}(v_y/v_x) \quad (9)$$

B. Drawbar pull and Side force

A general force model for a rigid wheel on loose soil is presented in Fig. 4. Using the normal stress $\sigma(\theta)$ and the shear stress in x direction $\tau_x(\theta)$, the drawbar pull F_x is calculated by the integral from the entry angle θ_f to the exit angle θ_r [3]:

$$F_x = rb\int_{\theta_r}^{\theta_f}\{\tau_x(\theta)\cos\theta - \sigma(\theta)\sin\theta\}d\theta \quad (10)$$

where, b represents a width of wheel.

The side force F_y acts along the lateral direction of a wheel when the vehicle makes a steering maneuver. We have modeled the side force as follows [4]:

$$F_y = \int_{\theta_r}^{\theta_f}\{rb\cdot\tau_y(\theta) + R_b\cdot(r - h(\theta)\cos\theta)\}d\theta \quad (11)$$

where, R_b is the reaction resistance generated by the bulldozing phenomenon on the side face of the wheel. R_b is given as a function of a wheel sinkage h. $\tau_y(\theta)$ is the shear stress in y direction.

C. Single Wheel Experiment

To validate the analytical model for wheel force, experiments using a single-wheel test bed are conducted. The experimental results are compared with the numerical simulation results obtained from the analytical model, and then, the characteristics of both the drawbar pull and side force are confirmed.

1) Single-wheel test bed: Fig. 5 shows the schematic view of the single wheel test bed. The test bed comprises both a conveyance unit and a wheel-driving unit. The steering angle (which is equivalent to the slip angle in this test bed) is set between the conveyance unit and the wheel. The translational velocity and angular velocity of the wheel are calculated based on the data obtained by the encoders that are mounted on the conveyance motor and wheel-driving motor, respectively. The forces and torques generated by the wheel locomotion are measured using a six-axis force/torque sensor located between the steering part and the wheel. In the

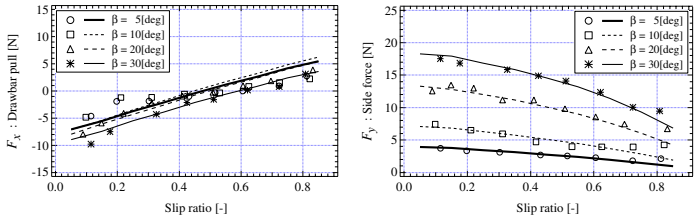

(a) : Drawbar pull (b) : Side force

Fig. 6. Experimental and simulation results

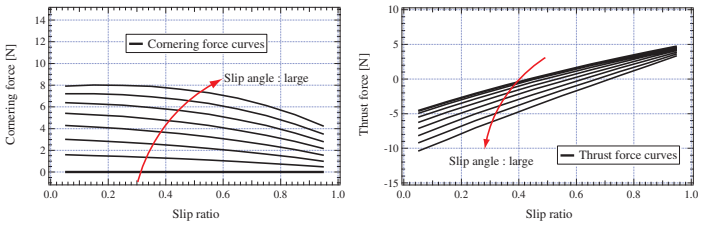

(a) : Cornering force (b) : Thrust force

Fig. 7. Characteristics of cornering and thrust forces

experiment, the vessel of the single-wheel test bed is filled with around 10 [cm] (depth) of loose sand, *Toyoura sand*, which is loose sand and standard sand for terramechanics research field. A wheel with a diameter of 110 [cm] and a width of 6.4 [cm] is covered with paddles having heights of 0.5 [cm]. The total load of the wheel is approximately 5.1 [kg].

In the following experiments, the wheel is made to rotate with a controlled constant velocity (0.015 [m/s]) by the driving motor mounted inside the wheel. The translational velocity of the wheel is also controlled such that the slip ratio of the wheel is set from 0.0 to 0.8 in steps of 0.1. The slip ratio is constant during each run. Further, the value of the slip angle of the wheel is varied from 5° to 30° in steps of 5°.

2) Experimental results: Experimental measurements of a drawbar pull and a side force are respectively plotted in Fig. 6, for each slip angle, 5, 10, 20, and 30 [deg]. Theoretical curves calculated by the analytical model are also drawn in the corresponding figures.

From Fig. 6, it is seen that the drawbar pull increases as the slip ratio increases, but it decreases as the slip angle increases. Also, the side force decreases along with the slip ratio and increases according to the slip angle. The differences between the measured forces and the theoretical values are comparatively small. These results validate that the analytical model for wheel force is able to represent the traveling behavior of slipping wheel and the contact forces with a reasonable precision.

IV. THRUST-CORNERING CHARACTERISTICS DIAGRAM AND TRAFFICABILITY ANALYSIS

In this section, first, characteristics of cornering force and thrust force are described, and then, the thrust-cornering characteristics diagram is proposed. The trafficability analysis using the proposed diagram is also addressed.

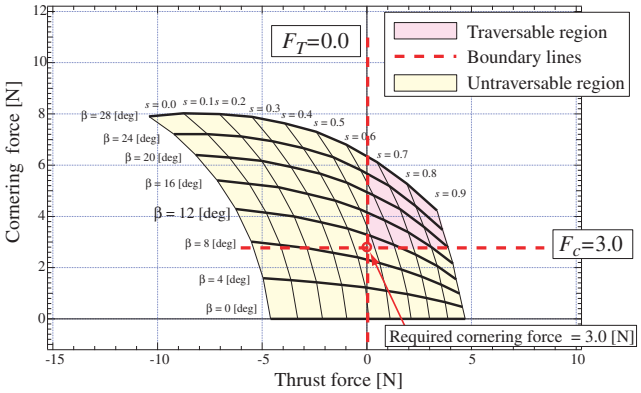

Fig. 8. Thrust-Cornering Characteristics Diagram

A. Thrust-Cornering Characteristics Diagram

The characteristics of both drawbar pull and side force for various wheel slippages has been clarified in Section III. Therefore, the characteristics of cornering and thrust forces with different slip ratios/slip angles can be elaborated as shown in Fig. 7.

In this research, we came up with the following approach: combining Fig. 7-(a) and (b), the relationship between the cornering force and thrust force can be obtained as a diagram as shown in Fig. 8. This diagram is proposed as Thrust-Cornering Characteristics Diagram.

B. Approach of Trafficability Analysis

The trafficability analysis using this diagram can be conducted as follows: First, a cornering force of each wheel which balances with a traction load on an arbitrary slope angle can be determined using (7). For instance, this cornering force is assumed to be around 3.0 [N]. Then, this turns out that the required cornering force to traverse the slope is given as $F_c \geq 3.0$. Also, referring to another criteria for slope traversing capability determined in (4), the required thrust force is given as $F_T \geq 0$. Subsequently, drawing these two boundary lines ($F_c \geq 3.0$ and $F_T \geq 0$) on the diagram, it can be seen that the diagram is divided into two regions, traversable/untraversable regions.

As shown in Fig. 3, if the rover successfully traverses the slope in straight ahead, the steering angle is assumed to be equivalent to the slip angle. Therefore, by calculating the thrust-cornering characteristics diagram, the trafficability of the rover with given steering angles is simply determined: for instance, as shown in Fig. 8, the rover having more than 12 [deg] of steering angles will be able to traverse and climb the corresponding slope since the characteristics curve of $\beta = 12$[deg] is larger than the required cornering force.

C. Slope Traversing Experiment

In order to validate the proposed diagram for the trafficability analysis, slope traversal experiments using a four-wheel test bed is carried out. In this paper, two cases are addressed; slope traversable and untraversable cases with changing slope angle.

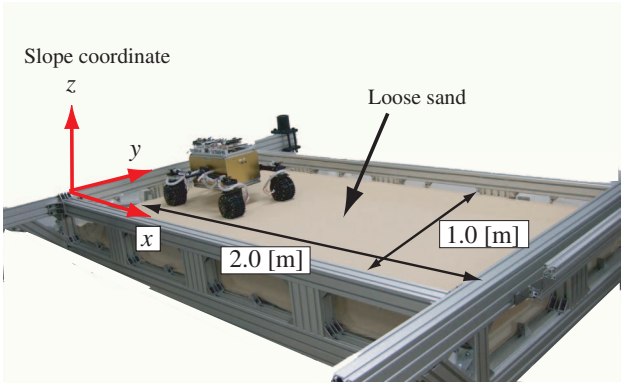

Fig. 9. Overview of the experimental setup

1) Experimental Setup: Fig. 9 shows the overview of the experimental setup with our rover test bed. The facility consists of a rectangular tiltable vessel in the size of 2.0 by 1.0 [m]. The vessel is filled up with 8.0 [cm] depth of Toyoura Sand. The four-wheeled rover test bed has a dimension of 0.44 [m] (wheelbase) $\times$ 0.30 [m] (tread) $\times$ 0.30 [m] (height) and weights about 13.5 [kg] in total. Each wheel of the rover is same as the one used in the single wheel experiment.

In the experiment, each steering angle of all wheels of the rover is controlled to maintain 15 [deg] to the uphill direction of the slope. The experiments are conducted in two cases: in case-A, the slope angle is 5 [deg], and in case-B, it is 10[deg].

2) Trafficability analysis using proposed diagram: The motion trace of the rover in these experiments are illustrated in Fig. 10. From the figures, the rover can successfully traverse and climb in case-A (the slope angle is 5 [deg]), however, the rover slid down the slope in case-B (10 [deg]). In this latter case, it is deduced that the summation of cornering forces must be smaller than the traction load of the rover.

This difference between traversable and untraversable can be explained by using the thrust-cornering characteristics diagram. The thrust-cornering diagrams for uphill/downhill wheels in case-A and case-B are shown in Fig. 11 and Fig. 12. A red circle in each diagram indicates the required cornering force calculated by (7). Also, a blue curve on the diagram denotes the specific thrust-cornering curve when the slip angles of wheels are 15 [deg].

From Fig. 11, it is found that the required cornering forces of both uphill/downhill wheels (red circles) are smaller than the specific thrust-cornering curves (blue curves) when $F_T = 0$. This means that wheels of the rover in case-A generate large enough cornering forces so that the rover can traverses and also climbs the slope. However, in case-B as shown in Fig. 12, the specific thrust-cornering curves in either uphill/downhill wheels never exceed the required cornering forces. Also, the curves never overlap into the traversable region at any slip ratios; therefore, the rover in case-B cannot traverse the slope.

The following point should be emphasized: the thrust-cornering characteristics diagram in case-B also indicates

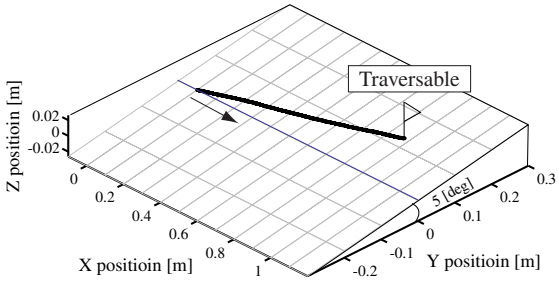

(a): case-A: slope angle 5 [deg]

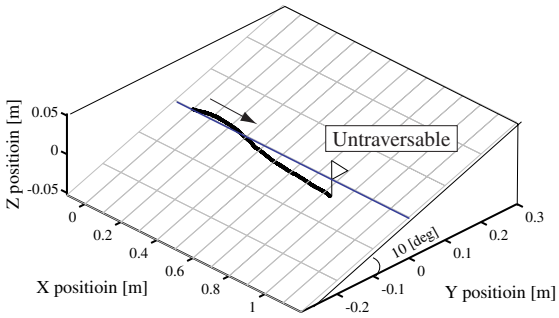

(b): case-B: slope angle 10 [deg]

Fig. 10. Slope traversing experiments

that the rover on the slope of 10 [deg] will be able to traverse the slope if the steering angle is given such that the specific thrust-cornering curve exceeds the required cornering force (i.e. appropriate steering angle will be around 20 [deg].)

V. POSSIBLE APPLICATION FOR STEERING MANEUVER

In this section, possible application using the thrust-cornering characteristics diagram is concisely addressed.

Through the trafficability analysis described in Section IV, it is found that the thrust-cornering characteristics diagram will be useful to determine appropriate steering angles for successful slope traversing. Also, as discussed in Section II, when a rover traverses a slope, there is an equilibrium point where a traction load is equal to a summation of cornering forces. Using this force equilibrium, the rover can traverse a slope along with straight line, or without any sideslip of vehicle. In this condition, a steering angle δ of wheel is equivalent to the wheel slip angle. Therefore, if the required cornering force for slope traversing is given, it is expected that an appropriate steering angle can be found as an intersection point where two boundary lines cross on the thrust-cornering characteristics diagram.

Based on this approach, a typical case study is addressed in this paper. Using the trust-cornering characteristics diagrams for case-B (Fig. 12), the steering angles, which correspond to the intersection point of two boundary lines, can be determined as 18.9 [deg] for uphill wheels and 19.5 [deg] for downhill wheels. Then, the slope traversing experiment with the derived steering angle to each wheel are conducted and the result is shown in Fig. 13.

From the figure, it can be seen that the rover in both cases can successfully traverses the slope. The error to the

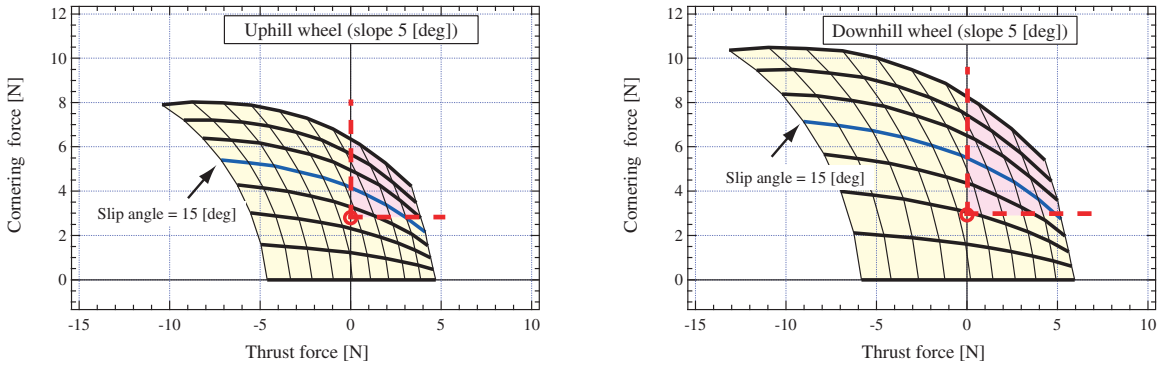

Fig. 11. Thrust-cornering characteristics diagram : case-A (slope angle is 5 [deg])

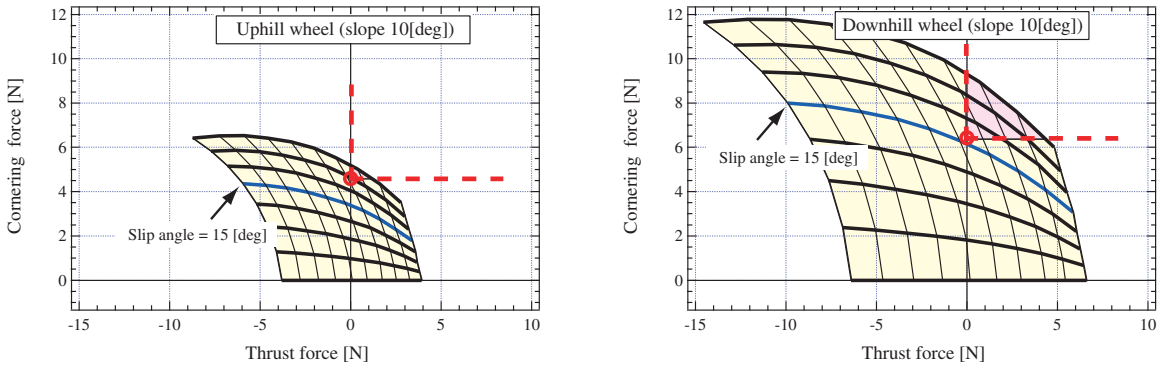

Fig. 12. Thrust-cornering characteristics diagram : case-B (slope angle is 10 [deg])

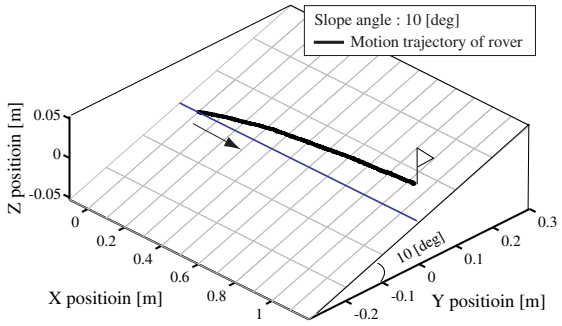

Fig. 13. Slope traversing with steering maneuver using proposed diagram

straight line indicated as a blue solid line in the figure is less than 7 [cm]. This error is due to an error regarding the analytical model for wheel force. However, the results indicate that the proposed diagram will be useful for a model-based feedforward control to traverse a sandy slope.

VI. CONCLUSION

In this paper, the trust-cornering characteristics diagram has been proposed for the trafficability analysis of the rover. This diagram provides quantitative criteria for slope traversing capability of the rover on arbitrary angles of slope. The usefulness of the proposed diagram has been confirmed through slope traversal experiments using a four-wheel test bed. Also, the possible application using the proposed diagram has been presented.

The proposed diagram can be extended to an applications, such as controlling the driving/steering motion of the vehicle to follow a given path by compensating for the wheel slippages, as concisely described in Section V. The trust-cornering characteristics diagram will be also useful in performing path planning computation of the vehicle under slipping/skidding conditions. For example, a planetary terrain surface can be classified according to its traversable or untraversable areas using the diagram.

REFERENCES

[1] http://marsrovers.jpl.nasa.gov/home/index.html (as of February 2008)

[2] M. G. Bekker; *Introduction to Terrain-Vehicle Systems*, The University of Michigan Press, 1969.

[3] J. Y. Wong; *Theory of Ground Vehicles*, John Wiley & Sons, 1978.

[4] G. Ishigami, A. Miwa, K. Nagatani, and K. Yoshida; "Terramechanics-Based Model for Steering Maneuver of Planetary Exploration Rovers on Loose Soil," *The Journal of Field Robotics,*, Vol. 24, No. 3, pp. 233-250, 2007.

[5] H. Seraji; "Traversability Index: A New Concept for Planetary Rovers," *Proc. of the 1999 IEEE Int. Conf. on Robotics And Automation,* pp. 2006-2013, 1999.

[6] Y. Kuroda, T. Teshima, Y. Sato, and T. Kubota; "Mobility Performance of Planetary Rover in Difference of Gravitational Acceleration," *Proc. of the 2005 IEEE/RSJ Int. Conf. on Intelligent Robots and Systems,* pp. 1413-1418, 2005.

[7] K. Yoshida, N. Mizuno, G. Ishigami, A. Miwa; "Terramechanics-Based Analysis for Slope Climbing Capability of a Lunar/Planetary Rover," *Proc. of the 24th Int. Symp. on Space Technology and Science,* 2004-k-06, 2004.